3D-printed chitosan-based scaffolds: An in vitro study of human skin cell growth and an in-vivo wound healing evaluation in experimental diabetes in rats

3D-printed chitosan-based scaffolds: an *in vitro* study of human skin cell growth and an *in-vivo* wound healing evaluation in experimental diabetes in rats

Claudio Intini[1,3], Lisa Elviri[1*], Jaydee Cabral[2], Sonya Mros[3], Carlo Bergonzi[1], Annalisa Bianchera[1], Lisa Flammini[1], Paolo Govoni[4], Elisabetta Barocelli[1], Ruggero Bettini[1], Michelle McConnell M[3]

[1]Food and Drug Department, University of Parma, Parco Area delle Scienze 27/A, 43124, Parma, Italy.

[2]Department of Chemistry, University of Otago, Dunedin 9054, New Zealand.

[3]Department of Microbiology & Immunology, University of Otago, Dunedin 9054, New Zealand.

[4] Department of Medicine and Surgery, University of Parma, Parma, 43124, Parma, Italy.

Lisa Elviri

[1]Food and Drug Department, University of Parma, Parco Area delle Scienze 27/A, 43124, Parma, Italy.

* Corresponding Author

E-mail: lisa.elviri@unipr.it

ABSTRACT

The fabrication of porous 3D printed chitosan (CH) scaffolds for skin tissue regeneration and their behavior in terms of biocompatibility, cytocompatibility and toxicity toward human fibroblast (Nhdf) and keratinocyte (HaCaT), are presented and discussed. 3D cell cultures achieved after 20 and 35 days of incubation showed significant *in vitro* qualitative and quantitative cell growth as measured by neutral red staining and MTT assays and confirmed by scanning electron microphotographs. The best cell growth was obtained after 35 days on 3D scaffold when the Nhdf and HaCaT cells, seeded together, filled the pores in the scaffolds. An early skin-like layer consisting of a mass of fibroblast and keratinocyte cells growing together was observed. The tests of 3D printed scaffolds in wound healing carried out on streptozotocin-induced diabetic rats demonstrate that 3D printed scaffolds improve the quality of the restored tissue with respect to both commercial patch and spontaneous healing.

Keywords: 3D printing, chitosan scaffold, chitosan biocompatibility, fibroblast and keratinocyte cells, skin tissue engineering.

1. Introduction

Tissue engineering is a promising field of regenerative medicine that relies on the interaction of three main elements: a supporting material, growth factors, and cells to develop a biological substitute for the replacement, restoration or regeneration of damaged tissues and organs (Khademhosseini, Vacant & Langer, 2009). The challenge of this matter is to mimic what happens in nature. Attempts are being made to engineer *in vitro* various tissues and organs. To date, the highest rates of success have been achieved in the areas of skin (Yannas, Lee, Orgill, Skrabut & Murphy, 1989), bladder (Atala, Bauer, Soker, Yoo & Retik, 2006), airway (Macchiarini, 2008), and bone (Schimmin & Schmelzeisen, 2004; Warnke, 2004), where tissue-engineered constructs have been successfully used in patients (Zhang, Kiu, Yang, Yao & Yao, 2017, Chen & Chang, 2012; Bello, Falabella & Eaglstein, 2001).

Focusing attention on skin tissue engineering, the production of extra-cellular matrix (ECM) plays a pivotal role in the regeneration process, driving cell proliferation, differentiation and maturation. Furthermore, ECM provides characteristics of storage and delivery of growth factors and cytokines and it supplies structural integrity and scaffolding features as *substratum* for glycosaminoglycans such as, hyaluronic acid (HA) and collagens, naturally secreted by recruited cells during initial phases of regeneration (Xue & Jackson, 2015).

A relevant task of skin tissue engineering is thus focused towards the bio-fabrication and use of porous three-dimensional (3D) scaffolds (Khademhosseini, 2009) as appropriate environments for cell colonization and proliferation, thereby enabling the production of ECM and the reconstruction of complex tissues.

Among the different scaffold preparation processes (Ho et al. 2004; Weigel, Schinkel & Lendlein 2006; Ko, Oh Kawazoe, Tateishi & Chen, 2011), 3D printing and bioprinting are innovative technologies drawing tremendous attention from both academia and industry for their potential applications in various fields, including regenerative medicine and pharmaceutical drug delivery. Biomaterials, biomolecules and/or cells are patterned by 3D advanced additive manufacturing

78 technologies to create scaffolds with arbitrary geometries and heterogeneous material properties,
79 which can mimic the complexity of native tissues (Azhari, Toyserkani & Villain, 2015). Although
80 3D bioprinting presents revolutionary capabilities, the design and fabrication of 3D devices are
81 critical. One of the key points is that scaffold constructs should address the needs for architecture
82 design at the macro, micro, and nano level involved in structural cell-matrix interactions and nutrient
83 transport (Karande, Ong & Agrawal, 2004; Stevens & George, 2005). Current 3D printing techniques
84 (i.e. extrusion printing, laser printing, droplet printing), are feasible to make accurate and rapid
85 fabrication of pre-designed structures with several natural (i.e. alginate, chitosan, collagen etc.) and
86 synthetic polymers (polylactide, polyethylene glycol, etc.) with resolution ranging from 20 μm for
87 laser techniques to 200-300 μm for the droplet and extrusion printing, respectively (Arslan-Yildiz et
88 al, 2016).
89 In the present work, an innovative extrusion-based 3D printing technique has been used for the
90 preparation of novel 3D chitosan scaffolds presenting controlled and reproducible macro- and micro-
91 structure to be applied in the regenerative skin tissue field (Bettini, Romani, Morganti & Borghetti,
92 2008; Elviri et al, 2017). This manufacturing approach combines the freeze-gelation method
93 described by Elviri *et al.* (2014) alongside an advantageous modification of the chitosan solution with
94 raffinose (Bettini, 2008) with the technical advantages of 3D printing. Chitosan (CH) is a natural
95 polysaccharide derived from the alkaline N-deacetylation of chitin, the main structural component of
96 the crustacean exoskeleton (Gasperini, Mano & Reis, 2014). When the number of N-acetyl-
97 glucosamine units is more than 50%, the biopolymer is referred to as chitin. Conversely, when the
98 number of N-glucosamine units is higher, the term chitosan is used. Chitosan has the potential to be
99 biocompatible, does not elicit adverse reactions in contact with human cells, is not allergenic and is
100 cheap (Galli et al 2016; Patil, Ghormade & Deshpande, 2000). It can be molded into a variety of
101 shapes, can be degraded by ubiquitous enzymes in the human body, and oligomeric products from
102 degradation can activate macrophages and stimulate synthesis of hyaluronic acid (Kumar, Muzzarelli,
103 Muzzarelli, Sashiwa, Domb, 2004; Peluso et al, 1994). Moreover, chitosan and chitin present

haemostatic action, which can be exploited to enhance healing (Okamoto et al. 1992). For these reasons, chitosan is one of the most investigated biomaterials for tissue engineering and bio-fabrication. In the last decade, several chitosan-based biomedical applications including wound dressing (Ueno et al. 1999; Mizuno et al, 2003), drug delivery (Ahn, Choi & Cho, 2001; Ahn, et al. 2002), and space filling implants (Zhao et al, 2002; Teng et al, 2002) have been successfully achieved. Presently, many chitosan-based medical devices are in clinical trials predominantly associated with bone, cartilage and skin tissue regeneration (Mekhail & Tabrizian, 2014).

Although many chitosan scaffolds have been studied in different cell cultures, the interactions of 3D printed constructs and cell behaviors is still under investigation as this is an important feature to be investigated before any *in-vivo* application.

In light of applications for chronic dermal wound treatments, in the present paper, the biocompatibility, cytocompatibility and toxicity of 3D printed chitosan scaffolds towards human skin cell lines were investigated. In our previously published paper (Elviri et al, 2017), the effect of a simple 3D printed architecture with 400 μm opening in scaffolds prepared by casting was demonstrated to significantly improve human fibroblasts adhesion and proliferation. In order to improve the understanding of the role of the third dimension on the accurate improvement of *in vitro* results, two different 3D scaffolds with 200 μm inter-filament opening were prepared (i.e. 3D printed scaffolds with or without the film of chitosan at the base) and individual and co-culture of fibroblast and keratinocyte cells were monitored.

In addition, in order to obtain evidence about the 3D scaffolds properties to improve tissue regeneration, these 3D scaffolds were assessed *in vivo* in a context mimicking a clinical feature using a model of wound healing in streptozotocin-induced diabetic rats.

2. Materials and methods

2.1. Materials

129 Chitosan ChitoClear® Fg90 TM4030 (CAS 9012-76-4, deacetylation degree 75%; molecular weight
130 by gel permeation chromatography 50-60 kDa; allergen free, water insoluble, soluble in acid media)
131 was from PRIMEX Ehf (Siglufjordur, Iceland).
132 Acetic acid 99.8% v/v, dimethyl sulfoxide (DMSO) and potassium hydroxide were from J.T. Baker
133 (Deventer, Netherland). Water was purified (0.055 uS/cm, TOC 1ppb) with a Purelab pulse + Flex
134 ultra-pure water system (Elga Veolia, Milan, Italy).
135 Neutral Red stain solution and MTT (3-(4,5-dimethylthiazol-2-yl)-2,5-diphenyl tetrazolium bromide)
136 reagent were purchased from Sigma-Aldrich (St. Louis, MO, USA). MTT reagent was dissolved in
137 water and stocked at concentration of 5 mg/mL; final concentration used was 1 mg/mL.
138

139 *2.2. 3D Printer*

140 A 3D home-made low temperature manufacturing system, built by combining Peltier cells and
141 liquid/air exchangers, was used at the laboratory scale through the insertion of bespoke modules in
142 the structure of a commercial Fuse Deposition Manufacturing (FDM) 3D printer. FDM architecture
143 is based on three Cartesian axes, two of which enliven the printing plate in x and y direction on the
144 horizontal plane, while the z-axis determines the progressive lifting of the extrusion nozzle. The
145 design of scaffold shapes was directly described by the geometric primitives of the axis control,
146 without need of translating them through general purpose programs for the transformation of the 3D
147 CAD model in a mesh to be subjected to slicing.
148

149 *2.3. 3D Chitosan scaffold fabrication*

150 All 3D chitosan scaffolds were constructed from a chitosan solution (6% w/v) in acetic acid 2% (v/v)
151 containing D-(+) raffinose pentahydrate at a final concentration of 290 mM. [18] The resulted
152 chitosan solution was treated in an ultrasonic bath for eliminating possible bubbles and clusters that
153 could cause processing problems, such as nozzle clogging during 3D printing process. Thereafter, the

154 solution was used to fill the 3D printer's cartridge, which was then assembled on the whole
155 equipment. The 3D printer was constituted by a mechanical apparatus that could be moved along the
156 three dimensions on axes-x, -y,-z, an extrusion system, composed in turn, by a syringe (volume 5
157 mL) and a needle (26 gauge), that could be assembled and disassembled, and a mobile plate on which
158 the solution was extruded and cooled at -14 °C with a series of Peltier cells. Several 3D chitosan
159 scaffolds were printed following the extrusion-based 3D printing process. The 3D matrices were
160 characterized from a projected area of 1 cm^2, a thickness of the first layer of about 0.3 mm and a
161 thickness of the other layers of about 0.2 mm for a total of 2.1 mm, and an opening of the network of
162 200 μm. Right after the 3D printing process, the scaffolds were gelled in potassium hydroxide KOH
163 8% (w/v) for 10 minutes and then stored in phosphate buffer saline PBS. This last passage was
164 necessary to increase the material rigidity for filament shape retention. A further, 3D chitosan
165 structure was produced which consisted of a compact chitosan film at the base to the previously
166 realized scaffolds. The purpose of this film was to occlude the lower base of scaffold to improve the
167 cell growth on it by keeping the cells inside. In detail, starting from the above-described chitosan
168 solution, the film was casted and uniformly spread on the plate of the 3D printer using a roll film,
169 before the printing process. After that, the 3D scaffold was printed above the film following the
170 already mentioned procedures.
171

172 *2.4. Mechanical resistance analysis*

173 The mechanical resistance of scaffolds obtained was calculated on 20-layers scaffolds having size of
174 5 cm x 1.5 cm. Thickness was determined as a mean of six measurements of the scaffold performed
175 with a digital micrometer (Mitutoyo, Japan). Each scaffold was fixed on a tensile tester (AG M1
176 Acquati, Italy) loaded with a 5 DaN cell. Force and time signals were digitalized by means of a
177 PowerLab 400 board and recorded with Scope 3.5 software. Elongation at break and Young's
178 modulus were determined from the relevant stress-strain curves.
179

2.5. Cell cultures

Normal dermal human fibroblast cells (Nhdf cells) and aneuploid immortal keratinocyte cells (HaCaT cells) obtained from American Type Culture Collection (ATCC®, Manassas, VA, USA) were used for *in vitro* tests.

Frozen stocks of these human cells at 1 x 10^6 cells/mL were initially put in 250 mL flasks, and sub-cultured in 750 mL flasks. Both cells were passaged in 750 mL flasks containing complete Dulbecco Modified Eagle Medium (DMEM, Gibco™, Thermo Fisher Scientific, Waltham, MA, USA) supplemented with 10% Fetal Bovine Serum (FBS, Gibco™, Thermo Fisher Scientific, Waltham, MA, USA) and 1% Penicillin and Streptomycin (PenStrep, Sigma-Aldrich, Saint Louis, MO, USA). Cells were incubated at 37 °C, 5% CO_2 in a cell culture incubator and were sub-cultured at 70% confluence.

2.5.1 3D Cell cultures

Fibroblast (Nhdf) and keratinocyte (HaCaT) cells were seeded individually at a concentration of 1x10^5 cells/mL on 3D chitosan scaffolds with or without the film of chitosan at the base; scaffolds were previous sterilized for 24 hours in 70% v/v ethanol. Each scaffold was inserted and seeded in a single well of a 12 or 24-well plate (Falcon® 12 or 24 Well Clear Flat Bottom TC-Treated Multiwell Cell Culture Plate, Corning®, New York, USA). Each plate's well was then filled with 1 mL or 2 mL of complete culture medium (DMEM, 10% FBS and 1% P/S) relative to whether the 12 or 24-well plate was used. The media was changed every 2 days in the first week of culture and every day in the remaining time of the experiment. When the cells were seeded together, Nhdf cells were added first on the scaffold in the specific well at 1 x 10^5 cells/mL concentration. Then, after one week, the culture medium was renewed and HaCaT cells at 2 x 10^5 cells/mL concentration were added. All 3D cell cultures were maintained in a 5% CO_2 incubator at 37 °C.

205 *2.5.2 Neutral red assay*

206 The Neutral Red assay (Babich & Borenfreund, 1990) was used to provide a qualitative estimation
207 on the presence of viable cells on 3D chitosan scaffolds at defined time points. The medium was
208 removed from the 3D cell cultures to be washed with PBS. Thereafter, the 3D chitosan scaffolds were
209 placed in a fresh plate in order to stain the cells growing on the scaffolds. The Neutral Red assay was
210 performed by adding 150 µL of Neutral Red solution (0.5% w/v) for each well. The cultures were
211 left in staining solution for 5 minutes at room temperature. They were washed two times carefully
212 and gently with PBS for 5 minutes each and at the end, 150 µL of PBS were added to each culture/well
213 before visualization. The results were observed under the transmitted light of an inverted microscope
214 (Leica DM IL, Bio-Strategy Ltd., Albany, New Zealand). Each completed assay corresponded to one
215 time point of analysis.

216

217 *2.5.3. MTT assay*

218 Fibroblast (Nhdf) and keratinocyte (HaCaT) cells seeded together on 3D chitosan scaffolds with and
219 without the film of chitosan at the base were analyzed after 2, 13, 20 and 35 days by means of a MTT
220 cell viability assay, as previously described (Favari et al, 2004). Using this method, the total number
221 of cells that were situated on the scaffold and on the plastic at the bottom of the well were quantitated.
222 In detail, at each time point, the medium was removed from the cultures, the 3D scaffolds were
223 washed once with PBS and inserted in a fresh well plate to be analyzed. 1 mL of MTT reagent solution
224 at concentration of 1 mg/mL dissolved in PBS was added to each well. The 12 or 24 well-plate was
225 then covered with aluminum foil as MTT is light sensitive, and was incubated at 37°C, 5% CO_2 for
226 1 hour. MTT reagent was also added to the original wells where the 3D chitosan scaffolds came from
227 in order to measure the cells grown on the bottom plastic surface of the well. Then, MTT solution
228 was replaced by pipetting 1 mL of acidified isopropanol, prepared by adding hydrochloric acid (37%
229 w/v) to isopropanol (1:1000 volume ratio) into each well. Finally, the plate was placed on a rotating
230 platform for 10 minutes at 100 rotation per minute to ensure complete solubilization of the formed

231 blue formazan crystals. The absorbance values were read at 570 nm using a Varioskan Flash
232 Multimode Reader (Thermo Fisher Scientific, Waltham, MA, USA). Different dilutions of the
233 samples, using acidified isopropanol solution, could be required depending on the viable cell numbers
234 expected. Each completed assay corresponded to one time point of analysis. Moreover, this assay was
235 also performed using two control groups, the 3D chitosan scaffolds only without cells, and cells only
236 without scaffolds.

237 *2.6. Scanning electron microscope (SEM) analysis*

238 Fibroblast and keratinocyte cells were seeded alone and together on both types of 3D chitosan
239 scaffolds. After 20 and 35 days, the cultures were fixed in 2.5% glutaraldehyde and in 0.1 M
240 cacodylate buffer for a total of 2 hours. They were then washed 3 times with PBS, post-fixed in 1%
241 osmium tetroxide, and in PBS for 1 hour. Then the samples were dehydrated in 30%, 50%, 70%,
242 80%, 95%, 100% v/v (the latter for 3 times) ethanol for 10 min each step and the Critical Point Drying
243 CPD (Bal-Tec AG, Balzers, Liechtenstein) was performed at 31°C. Then, the 3D chitosan scaffolds
244 were mounted on 12.5 mm aluminum stubs using double sided carbon tape and carbon paste and
245 coated with 10 nm of gold palladium for SEM viewing. 3D cell cultures were visualized with a
246 scanning electron microscope (Zeiss Sigma VP, Carl Zeiss, Oberkocken, Germany), at several
247 magnification values, EHT 1.00 kV and analyzed by Image J software (NIH, Bethesda USA).
248

249 *2.7.* In vivo *wound healing studies*

250 *2.7.1 Induction of diabetes in rats*

251 Research protocols were approved by the Italian Ministry of Health (D.Lgs 26/2014 ex D.Lgs.116/92)
252 and the experiments were carried out in compliance with the Guide for the Care and Use of Laboratory
253 Animals published by the US National Institutes of Health.
254 Adult female Wistar rats, weighing 250 to 350g, were used in this study. The animals were kept in

environmentally controlled rooms (22° ± 2°C, humidity 55±10%, 12 h light and dark cycle). The animals were allowed to take normal rat feed (reference laboratory food pellets (4RF21, Mucedola Srl, Settimo Milanese, Italy) and drinking water without restriction.

After an overnight fast, all animals (n=25) received an intraperitoneal injection of streptozotocin (50mg/kg; Sigma-Aldrich). Streptozotocin induces diabetes within 3 days by destroying the pancreatic β-cells; therefore 72h after injection, blood glucose was measured in overnight fasting animals. STZ-treated rats with whole-blood glucose levels higher than 250mg/dL were considered diabetic and used in the study. Fasting blood glucose was determined every 7 days throughout the experimental time to confirm the diabetic state, that leads to a delay in the time of wound healing with respect to physiological conditions. Rats were kept in cages individually, under feeding and drinking control: they were weighed daily and food and water consumption were measured.

2.7.2 Creation of skin wounds and treatment with 3D chitosan scaffolds

Three days before wounding, the dorsal interscapular area of each rat was depilated by a shaver and depilatory cream. On the day of wounding the rats were anaesthetized by intraperitoneal injection of 50 mg/kg ketamine and 5mg/kg xylazine. The operative area of skin was cleaned with chlorhexidine. A punch biopsy instrument (diameter 8mm) was used to create two full-thickness round wounds in the interscapular region of the upper back of each rat, and the skin flap was excised by using iris scissors. During the procedure particular attention has been placed to avoid incision of the muscle layer.

Rats were randomly assigned to two independent groups: Group 1 (n=13), with one wound covered with the 3D chitosan scaffold and the other one with a commercial product (positive control), Group 2 (n =12) with one wound covered with the 3D chitosan scaffold and the other one bare (negative control). In this way, according to 3R principles, each of the two groups had its internal control: in Group1 3D chitosan scaffold was compared to commercial product and, in Group 2, 3D chitosan

scaffold was compared to the absence of treatment. The wounds were additionally covered with dry cotton gauze and with adhesive film as a secondary dressing. All dressings were fixed with an elastic adhesive bandage. The rats were housed individually in large raised bottom mesh cages with free mobility. In the first week after the surgical procedure animals daily received paracetamol (100 mg/kg) in drinking water in order to alleviate discomfort and pain.

2.7.3 Wound closure evaluation

After 7, 10 or 14 days animals were sacrificed by CO_2 inhalation. The degree of wound healing was determined measuring the area of the wound with respect to a ruler by means of Image J software (https://imagej.nih.gov/ij/index.html) on photos of wounds taken at sacrifice. The percentage of wound contraction was calculated using the following formula (Karri et al, 2016):

$$\text{Wound contraction (\%)} = \frac{\text{Initial wound area} - \text{wound area on the n}^{\text{th}}day}{\text{initial wound area}} \times 100$$

After animal sacrifice, samples were excised from the area of the wound and immediately fixed in PBS-buffered paraformaldehyde at pH 7.4. Samples were then embedded in paraffin for sectioning using a microtome; slices of 6 um were cut and stained with hematoxylin-eosin, with the addition of sirius red to measure collagen distribution. Images were taken using an optical microscope Nikon Eclipse 80i, equipped with a camera Nikon Digital Sight DS-2Mv and connected to the control software, NIS Elements F (Nikon Instruments, Italy).

2.8 Statistical Analysis

Results were expressed as mean ± standard deviation (SD). Paired Student's t-test was used for analysis of data within each group of STZ-teated rats or one-way analysis of variation (ANOVA) was used for comparison of the experimental groups to a control group. A value of $p<0.05$ was considered statistically significant.

3. Results and discussion

3.1 Preparation of 3D printed chitosan-based scaffolds and cell adhesion study

In order to properly evaluate, through qualitative and quantitative analysis, the formation of multi-layered, high-density cell populations in 3D scaffolds a highly reproducible and defined 3D printing process should be used. The preparation and characterization of the 3D printed scaffolds employed in this study was described by Elviri *et al* (Elviri, Bianchera, Bergonzi &Bettini, 2016). These scaffolds were characterized by an accurate geometry and good surface homogeneity in terms of pore size and distribution: on the surface of the filaments the pores (Feret diameter: 3.5 ± 3 μm) presented a preferential orientation, whereas regular interconnected and layered pore structure (Feret diameter: 5 ± 4 μm) within the filaments, were observed by SEM analysis. [19] Whereas the scaffold dehydration process causes a reduction in its size of about 45%, pore size ranges from 4 to 9 μm which could be beneficial for cell adhesion and migration.

As described in Materials & Methods section, mechanical resistance of scaffolds was measured with the help of a tensile tester. Young's modulus was calculated and resulted 105 kPa ± 18 kPa (n=6). As reported by Liang and Boppart (Liang & Boppart, 2010), these values of elastic moduli are comparable to those observed in skin, in particular in volar forearm region. This suggests that if applied as wound healing patch, this could be integrated into wound and adapt to it.

All further experiments herein described were carried out using 3D printed chitosan-scaffolds patterned with a 200 µm geometry with and without a chitosan film at the bottom (Figure 1 A-B).

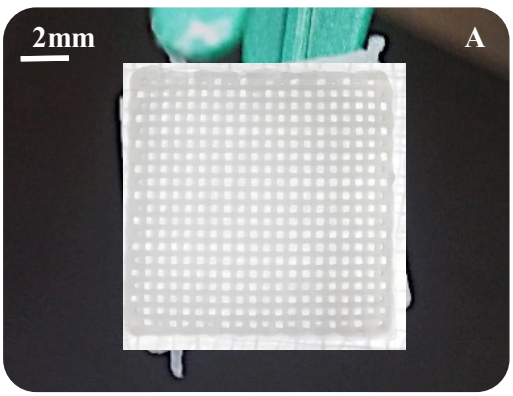

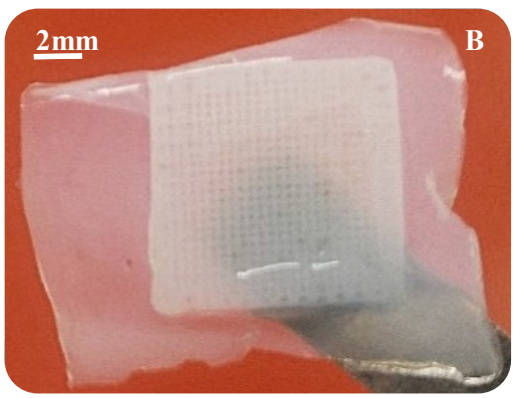

Figure 1. Photographs of the 3D chitosan scaffold without (photograph **A**) and with (photograph **B**) a film of chitosan at the base.

Keratinocyte visualization by optic light or scanning electroscope microscopy on the 3D scaffolds from the bottom to the top was easier than that of fibroblasts, due to the geometry of these cells. Keratinocytes appeared as a ball with a rounded shape (Figure 2A) possessing a diameter of approximately 20 µm, in agreement with the literature (Barrandon & Green, 1985). Fibroblasts, on the other hand, appeared elongated (about 50-100 µm length) and extremely thin, and for this reason were harder to visualize (Figure 2B). Moreover, all neutral red and scanning electron microphotographs posted in this work were collected and scanned from the top to the bottom part of the 3D scaffold.

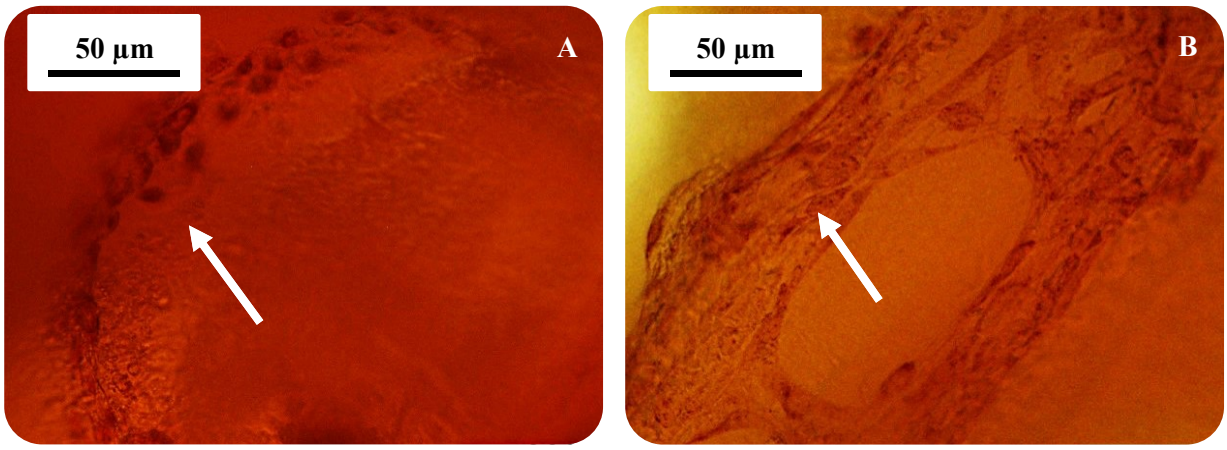

Figure 2. Microphotographs showing the differences of cell's shape between keratinocyte (**A**) and fibroblast (**B**) on 3D chitosan scaffolds upon Neutral Red staining.

By testing 3D chitosan scaffold without and with a film of chitosan at the scaffold bottom, it was possible to provide evidences of how fibroblast and keratinocyte cells were able to attach, live and grow after 20 days (Figure 3).

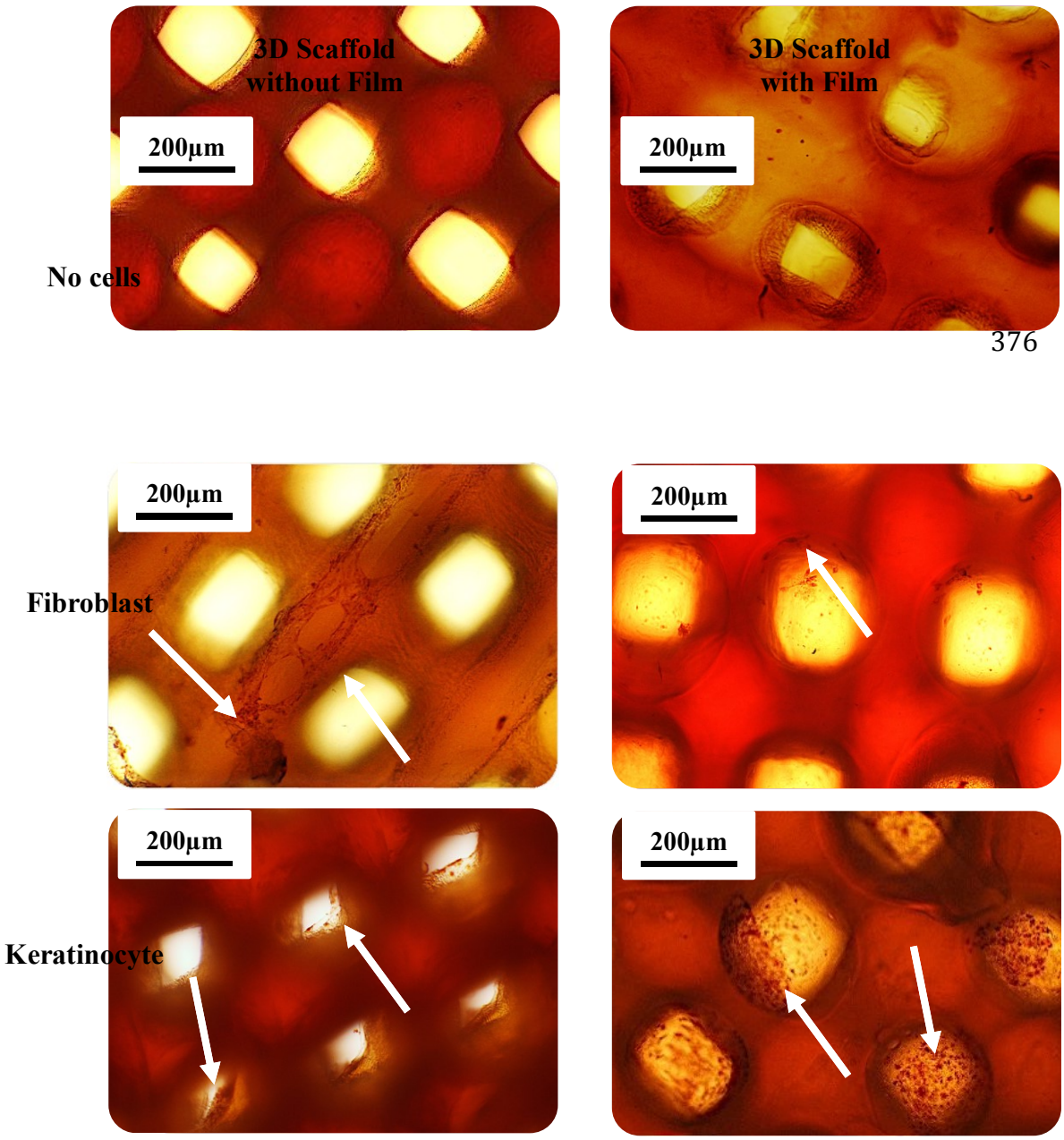

Figure 3. Microphotographs of Nhdf and HaCaT cell growth going after 20 days on 3D chitosan scaffolds with and without the chitosan film at the base upon Neutral Red staining.

All parts of the scaffolds, on the filaments, inside the holes and on the planar substrate, seemed to be biocompatible with no toxicity observed towards the analyzed cell's phenotypes and appeared to be suitable to support colonization. These results indicated that the tested chitosan hydrogel was a

suitable substrate for cell growth, in agreement with previous findings by Galli *et al.* (2016) and Bettini *et al.* (2008). Furthermore, Figure 4 (A-C) displays how the cells were able not only to grow on the structures, but also to fill the holes from the bottom to the top part of the scaffold trying to colonize the whole substrate. The best colonized scaffolds were observed with HaCaT cells seeded alone and analyzed after 20 days, as well as with Nhdf and HaCaT cells together after 35 days, in both cases on the 3D chitosan scaffolds with the film at the bottom (Figure 4 D-E).

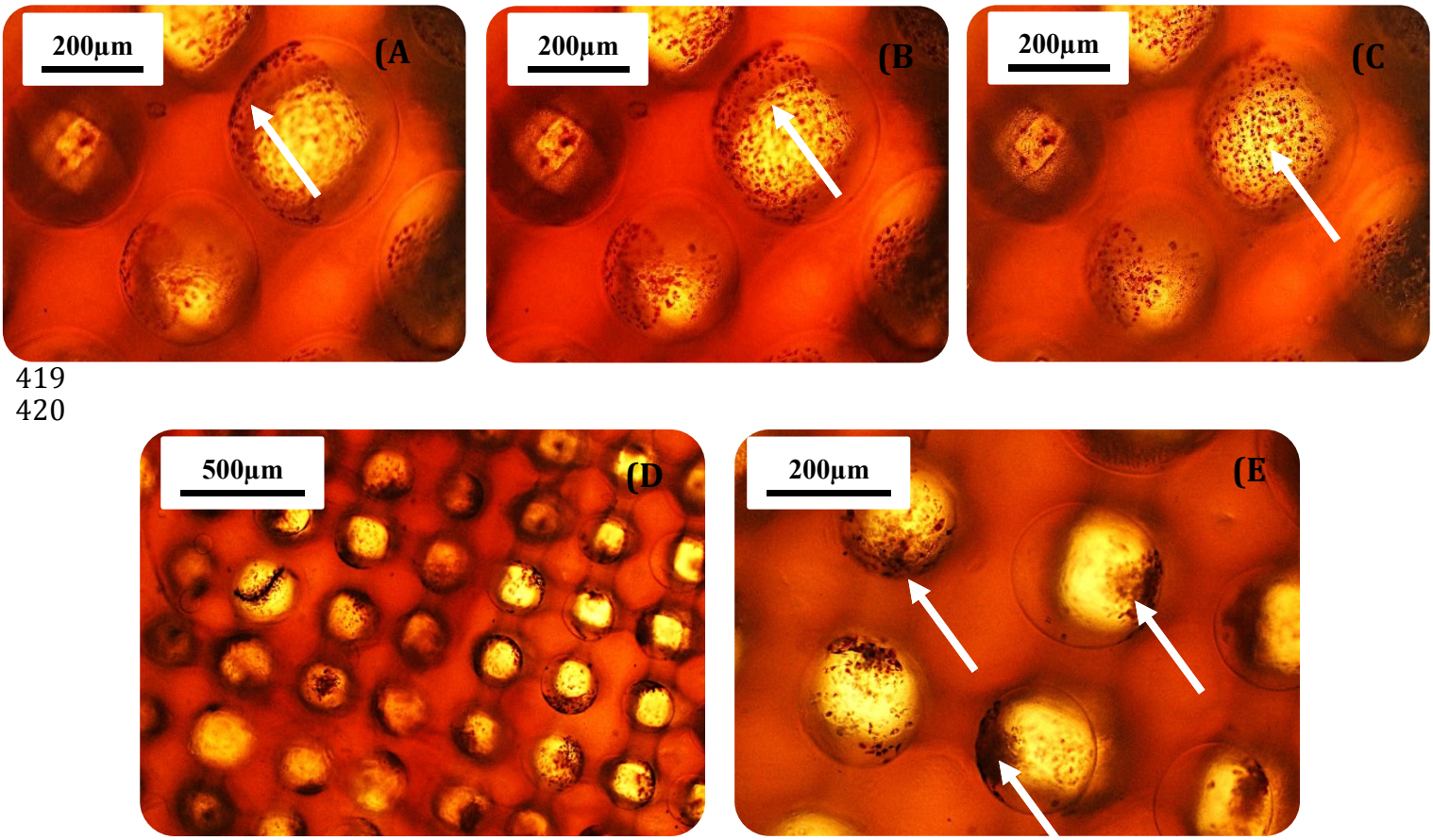

Figure 4. (A-B-C) Microphotographs taken at three different focal points (from left to right > depth) of HaCaT cells seeded on 3D chitosan scaffolds with the film of chitosan at the base and processed after 20 days upon Neutral Red staining. **(D-E)** Microphotographs of Nhdf and HaCaT cell after 35 days seeding them together on 3D chitosan scaffolds with the film of chitosan at the base upon Neutral Red staining.

428 In Figures 3 and 4, it was evident how the cells filled partially or completely the top part of the film
429 and the walls of the holes. HaCaT and Nhdf cells seeded together exhibited the best situation likely
430 because they can collaborate with each other releasing useful growth's factor for improving growth
431 and vitality (Barrandon, 1985). Moreover, it was also clearly appreciable how the presence of the
432 film on the base of the 3D structure resulted in a significant improvement in keeping the cells inside
433 the scaffold. A further evidence provided by this assay was that the fibroblast growth appeared
434 visually slower than that of keratinocytes. This can be clearly seen in Figure 3 depicting Nhdf and
435 HaCaT cells, taken at the 20 day time point after individual seeding. This finding was taken into
436 consideration for setting up the next experiment where a higher starting number of fibroblast with
437 respect to keratinocytes cells was used.
438
439 *3.2. Cell viability analysis*
440 Cell viability was evaluated by measuring the activity of the mitochondrial enzyme succinate
441 dehydrogenase by MTT test as previously described. Only the best experimental condition obtained
442 by the Neutral Red analysis, namely, fibroblast (Nhdf) and keratinocyte (HaCaT) seeded together on
443 3D chitosan scaffold, was evaluated. The MTT assay confirmed the neutral red assay results showing
444 how the chitosan substrate was not cytotoxic and that the cells were viable and able to grow and
445 colonize 3D chitosan matrices. The graph in Figure 5A displays a significant presence and a steady
446 increase of metabolically active cells on 3D chitosan scaffolds analyzed between 2 and 35 days for
447 both structures without (2-35 days +38%; $p<0.001$) and with film (2-35 days +16%; $p<0.001$) (3D
448 chitosan scaffolds without film percentage increase: 2-13 days +18%; 13-20 days +13%; 20-35 days
449 +3%) (3D chitosan scaffolds with film percentage increase: 2-13 days +1%; 13-20 days +5%; 20-35
450 days +9%). Furthermore, it is worthy highlighting that the amount of metabolically active cells on
451 the scaffolds with film was significantly higher than without at every time point sampled. These data
452 clearly suggest how cell colonization on 3D chitosan scaffold with a film at the bottom can
453 significantly improve growth (percentage increase: 2 days +88%, $p<0.01$; 13 days +62% $p<0.0001$;

20 days +50% $p<0.0001$; 35 days +58% $p<0.0001$). 3D scaffolds with film kept higher number of cells on the structures but after 2 days a lower cell growth was measured in comparison with the structures without film. Instead, the graph in Figure 5B shows the comparison of cell growth between 2D and 3D structures and demonstrates how cells exploit the advantages of more complex constructs. The total amount of metabolic active cells adhered on the 3D scaffolds or located at the bottom of the well where they came from was measured and represented on the graph. After 13 days in the 2D environment the cells reached the maximum confluence inhibiting cell growth, and remained almost constant during the later time points (13-20 days -2%; 20-35 days +2%). Contrariwise on the 3D substrate, the cell growth continued until 35 days for both experimental conditions assessed (3D chitosan scaffolds without film: 13-20 days +10%; 20-35 days +12%) (3D chitosan scaffold with film: 13-20 days +19%; 20-35 days +27%) even though the amount of active cells after 13 and 20 days was lower than that measured on the 2D configuration (Figure 5B). The rate of 3D growth is slower due to the 3D scaffold surface topography, which may reduce cell-to-cell signaling as cells are not interconnected in a single monolayer as they are in the 2D system.

Instead, after 35 days the total number of metabolically active cells in to the 3D environments was comparable (3D scaffolds without film: 13 days -24% $p<0.0001$; 20 days -15% $p<0.01$; 35 days -7% $p<0.05$) or higher (3D scaffolds with film: 13 days -28% $p<0.0001$; 20 days -12% $p<0.05$; 35 days +10% $p<0.01$) with respect to the corresponding value to 2D at the same time point. These results demonstrated that in both conditions the 3D environment positively stimulated cell colonization and growth. Again, 3D chitosan scaffold with film seeded with both cell's phenotypes afforded the better results.

Furthermore, the graph in Figure 5A, shows a slight increase in optical density values of the cultured scaffold relative to 3D scaffold without cells after 20 and 35 days (+1 fold and +3 fold to 3D chitosan scaffolds without and with film). This supports the previous hypothesis, as this increase could be ascribed to the absorbance of the oligosaccharides stemming from the chitosan degradation.

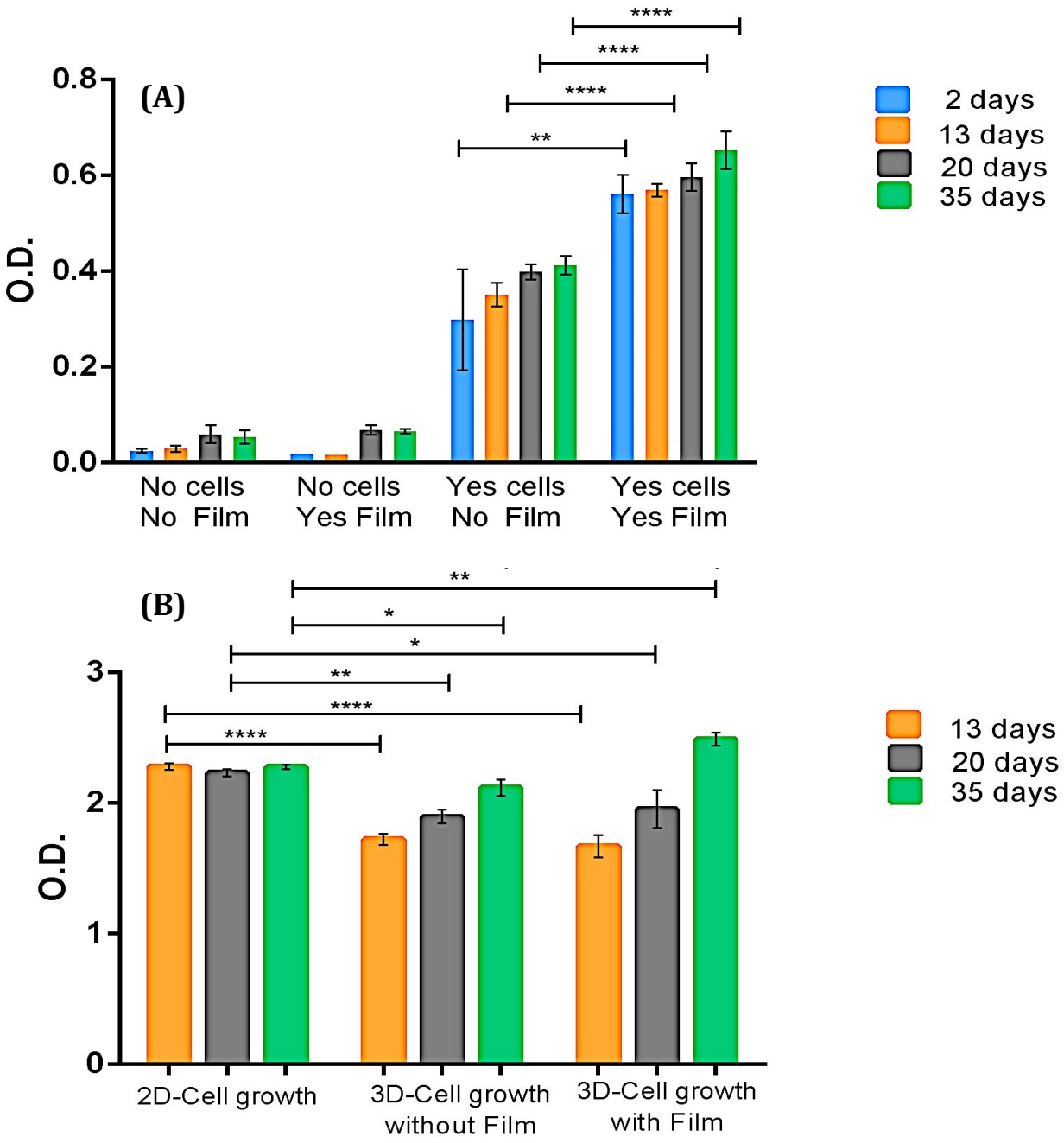

Figure 5. (A) Optical Density measured in MTT assays on Nhdf and HaCaT cells seeded together on 3D chitosan scaffolds. O.D. values are an average of triplicate readings. ** $p<0.01$; **** $p<0.0001$.

1. No Cells No Film = Only 3D chitosan scaffold without film; 2. No Cells Yes Film = Only 3D chitosan scaffold with film; 3. Yes Cells No Film = Cells and 3D chitosan scaffolds without film; 4. Yes Cells Yes Film = Cells and 3D chitosan scaffolds with film. (B) Comparison between two-dimensional and three-dimensional cell growth. The O.D. values of the total number of cells in wells are represented on the y-axis, three different time points are shown on the x-axis. O.D. values are an average of triplicate readings. * $p<0.05$; ** $p<0.01$; **** $p<0.0001$.

Three experimental conditions are reported: 1. 2D-Cell growth = Cells seeded in wells without 3D structures; 2. 3D-Cell growth without Film = Cells seeded in wells with 3D chitosan scaffolds without film; 3. 3D-Cell growth with Film = Cells seeded in wells with 3D chitosan scaffolds with film.

3.3. SEM analysis

Scanning electron microphotographs confirmed the successful colonization of the 3D structures. Again, the best results appeared to be those obtained with Nhdf and HaCaT cells seeded together on 3D chitosan scaffold printed with the film at the bottom. Figure 6, clearly shows the difference of colonization on the 3D structures in 20 and 35 days. In particular, after 20 days only a few clusters of cells were spread on the surface areas of 3D scaffolds, whereas after 35 days the cells had filled the scaffolds and closed the gap between the previous clusters, reinforcing scaffold biocompatibility (Figure 9B-C). In addition, SEM images captured from the bottom side of the structures without film, shows how the cells were able to build and develop an early skin-like layer, consisting of a mass of fibroblast and keratinocyte cells growing together. The lower surface of the scaffolds was completely covered by both cell's phenotypes that in some cases were organized in several areas resembling a protruding cluster or filopodia.

511

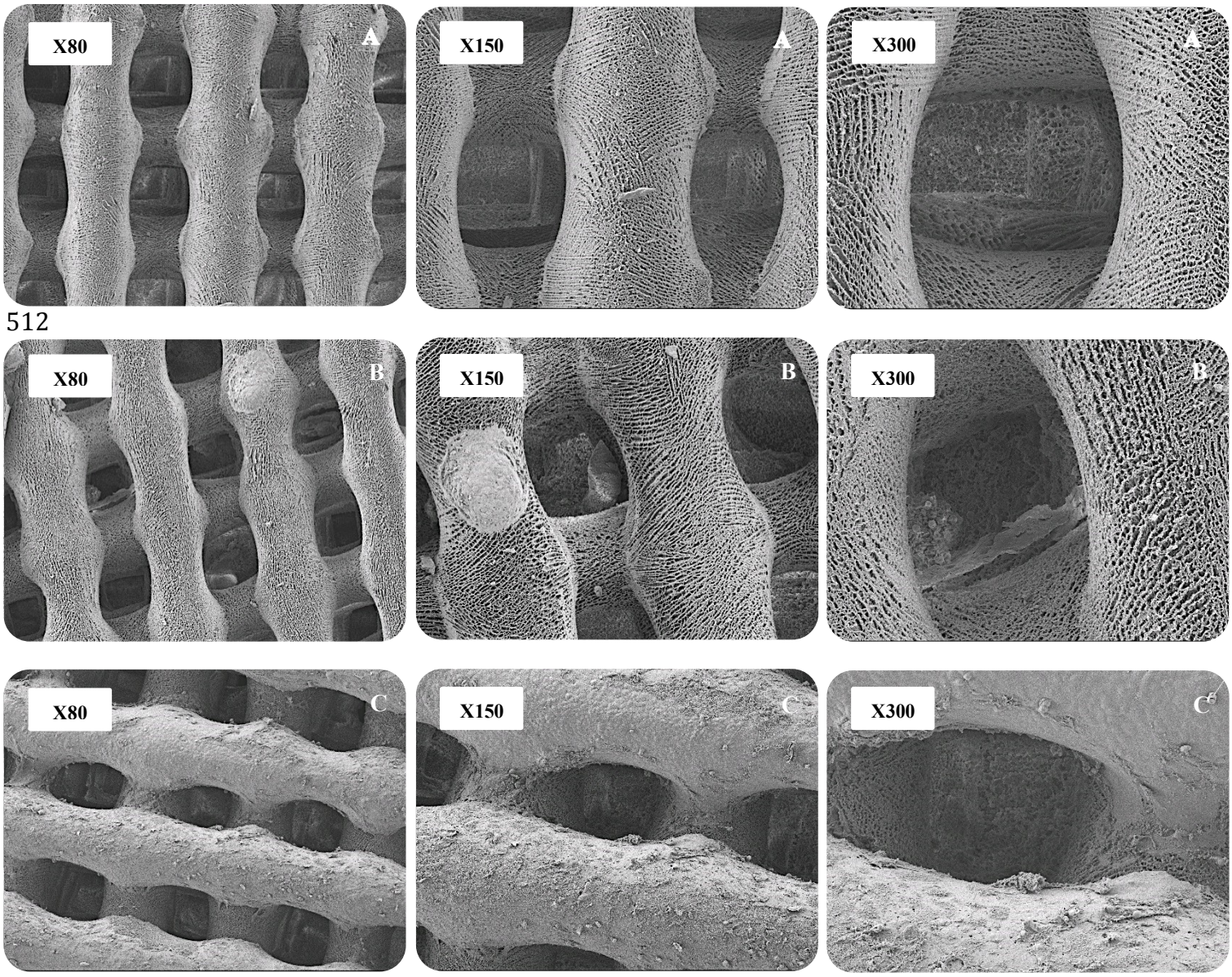

512

513

514 **Figure 6.** Scanning electron microscope photographs of Nhdf and HaCaT cells seeded together on
515 3D chitosan scaffolds with a film of chitosan at the base. Condition **A** represent the control scaffold
516 without cells, **B** scaffold with cells visualized after 20 days and **C** scaffold with cells after 35 days.

517

518 *3.4.* In vivo *test*

519 STZ-treated rats having stable hyperglicaemia were selected for these experiments as a model of
520 impaired wound healing. Images of wounds at day 7, 10 or 14 were taken and measured to estimate

521 wound contraction. As shown in figures 7a, starting from round excisions having an area of about 0,3
522 cm^2, seven days later, in animals treated with chitosan scaffolds or untreated ones, wounds appeared
523 reduced of about 50 % with respect to initial area (chitosan scaffold: 52±21%); control group 46
524 ±35%), while a more consistent, although not significant ($p>0.05$) contraction in wounds treated with
525 the commercial product was observed (reduction to about 20±17%): in all cases an extremely high
526 variability among animals was present. After 10 days, healing could be considered completed in
527 animals treated with chitosan scaffolds or commercial product, while in control animals scabs were
528 still present. After 14 days, all wounds were completely healed and only scars were visible.
529 Representative images of wounds at different time points are collected in figure 7b. On the whole,
530 visual inspection of wounds confirmed that treatment with chitosan scaffolds improved and
531 accelerated wound healing with respect to untreated animals, but did not show significant differences
532 with respect to the use of a commercial product: it is worth mentioning that in some cases, the use of
533 the commercial product lead to infection in wounds, while no signs of infection were observed on
534 any animal treated with chitosan scaffolds, probably thanks to its intrinsic antimicrobial activity.

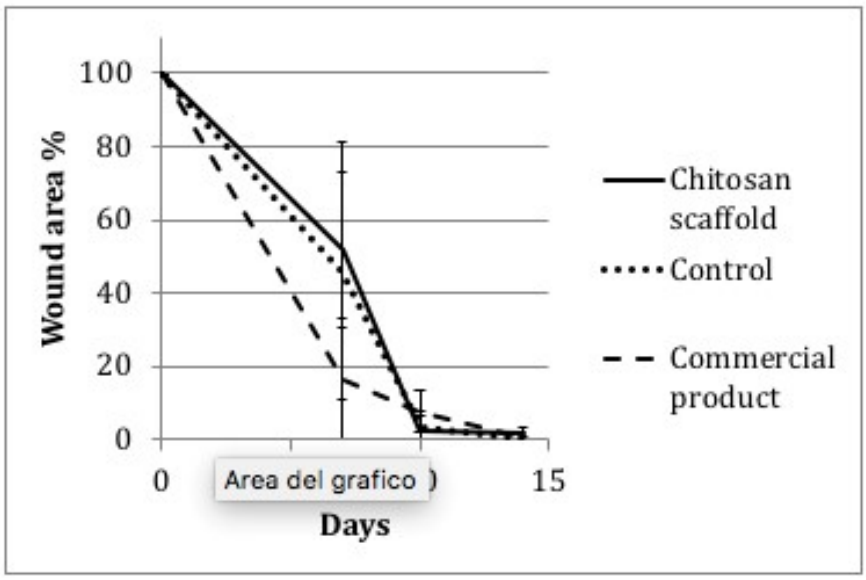

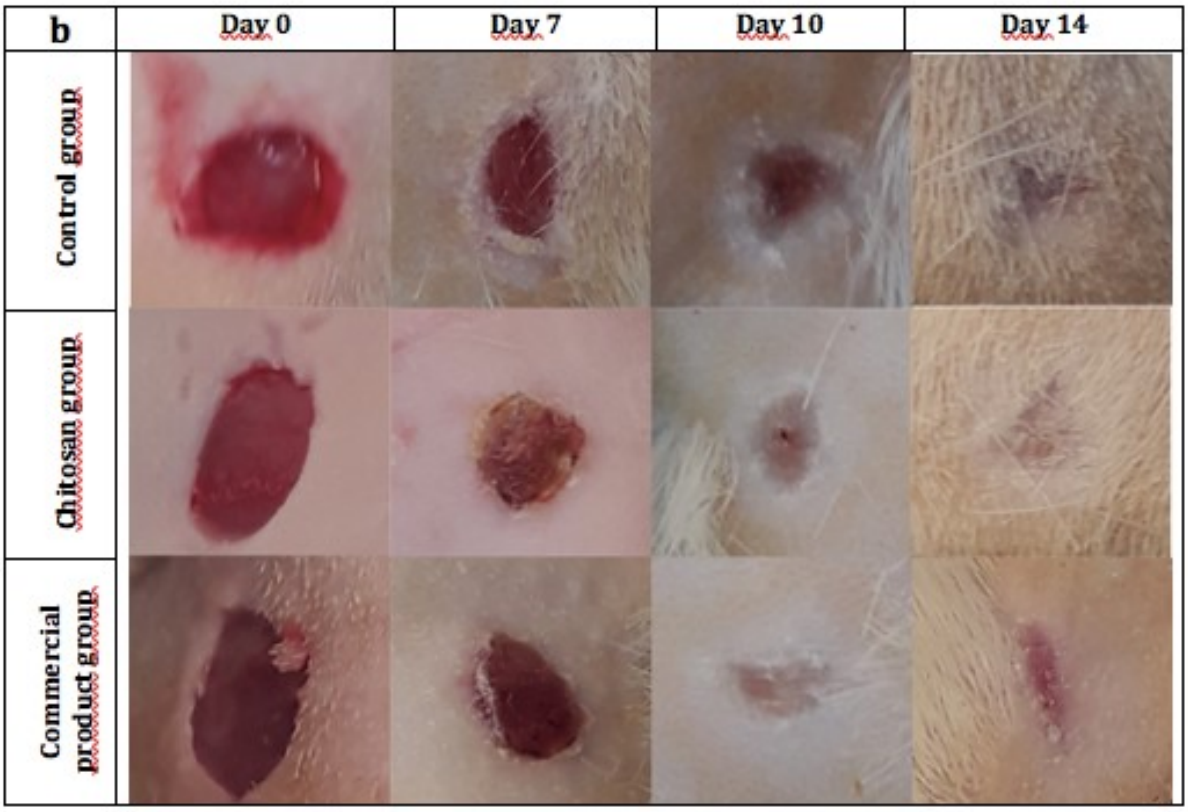

Figure 7. (a) contraction of wounds expressed as percent of inital area 7, 10 or 14 days after wound infliction; (b) representative images of wound healing in treated and untreated groups: each photo corresponds to an area of 1 cm^2.

Apart from macroscopic appearance, some differences in the quality of wound healing could be appreciated by histological analysis. Figure 8 shows the comparison of a wound treated with chitosan hydrogel (left) with respect to spontaneous healing (right), 7 days after wound infliction. The scarlet area on the side of both images marks the limit of original wound, evidencing collagen structure. In figure on the left, the intense purplish red area is indicative of a more intense tissue reorganization, with respect to the pale pink area of the photo on the right, were tissue organization and collagen is very scarce. Epidermis (purple layer up) is present only in the wound treated with chitosan hydrogel. In both images, healing is still ongoing, but the tissue formed on the wound treated with chitosan scaffold has a more mature appearance.

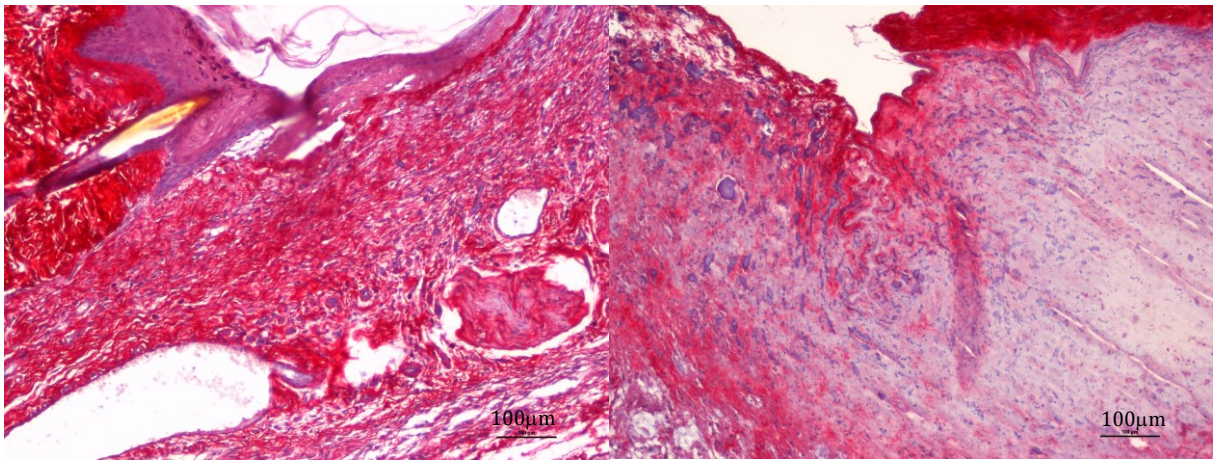

Figure 8. Histological staining H&E + sirius red of tissue excised from wounds treated with chitosan hydrogels (left) or spontaneously healed (right) for 7 days.

Figure 9 shows the comparison of a wound treated with chitosan hydrogel (left) with respect to a commercial product (right), 14 days after wound infliction. On the left, it is not possible anymore to distinguish the site of wound infliction, since the tissue is completely reorganized and the epidermis repaired (purple layer up), with a huge amount of collagen (scarlet red) that is not coarse anymore but rather mature and organized into fibrils. Moreover, tissue annexes are present such as blood vessels (v), sebaceous glands (g), hair follicles (h) and erector pili muscles (p). On the other hand,

figure on the right shows a wound treated with the commercial product: resulting tissue shows a non-ordered distribution of loose collagen fibers surrounding an area of tissue, that appears like fat tissue, with a functionality that is still compromised and without evidence of tissue annexes.

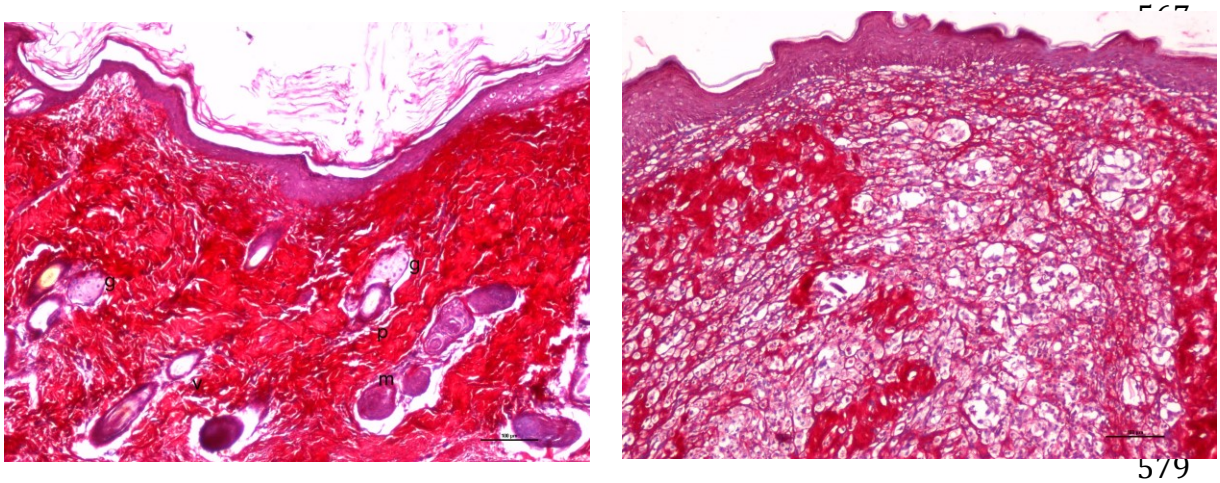

Figure 9. Histological staining H&E + sirius red of tissue excised from wounds treated with chitosan hydrogels (left) or a commercial product (right) for 14 days.

4. Conclusions

3D chitosan bio-polymeric scaffolds were fabricated using a newly developed extrusion-based 3D printing technique. This system provided a tool for precisely controlling the final shape and spatial distribution of the 3D chitosan structures.

These scaffolds exhibit excellent properties in terms of biocompatibility, cytocompatibility and toxicity toward two different skin associated human cell lines, namely Nhdf and HaCaT. These cell lines successfully attached, grew, and colonized the 3D structures. The best results were obtained when the two cell lines were seeded together onto 3D chitosan scaffolds with chitosan films at the base. Proliferating cells adhere and spread on the chitosan scaffold where interconnected cells form a continuous layer, which is significant for potential application in skin integrity restoration. Moreover *in vivo* tests on rat models of diabetes showed that the use of chitosan scaffolds to treat

595 wounds leads to a reduction in the time of healing with respect to untreated ones but, more important,
596 promotes the regeneration of a tissue with an improved functionality with respect to wounds treated
597 with a commercial product, suggesting the usefulness of chitosan scaffolds for the treatment of
598 chronic dermal wounds.
599
600

601 # References

602 Ahn JS, Choi HK, Cho CS. (2001) A novel mucoadhesive polymer prepared by template
603 polymerization of acrylic acid in the presence of chitosan. *Biomaterials* 22, 923–8.
604 Ahn JS, Choi HK, Chun MK, Ryu JM, Jung JH, Kim YU, Cho CS. (2002) Release of
605 triamcinolone acetonide from mucoadhesive polymer composed of chitosan and poly (acrylic
606 acid) in vitro. *Biomaterials* 23, 1411–6.
607 Arslan-Yildiz A, El Assal R, Chen P, Guven S, Inci F, Demirci U. (2016) Towards artificial
608 tissue models: past, present, and future of 3D bioprinting. *Biofabrication* 8,1-8.
609 Atala A, Bauer SB, Soker S, Yoo JJ, Retik AB. (2006) Tissue-engineered autologous bladders
610 for patients needing cystoplasty. *Lancet* 367, 1241-6.
611 Azhari A, Toyserkani E, Villain C. (20159 Additive manufacturing of graphene–
612 hydroxyapatite nanocomposite structures. *Int J Appl Ceramic Technol* 12, 8-17.
613 Babich, H. & Borenfreund, E. (1990) Applications of the neutral red cytotoxicity assay to in
614 vitro toxicology. Altern. Lab. Anim. 18, 129–144
615 Barrandon Y and Green H. (1985) Cell size as a determinant of the clone-forming ability of
616 human keratinocytes. *PNAS* 82, 5390-5394.
617 Bello YM, Falabella AF, Eaglstein WH. (2001) Tissue-Engineered Skin. *American Journal*
618 *of Clinical Dermatol* 2, 305-313.
619 Bettini R, Romani AA, Morganti MM, Borghetti AF.(2008) Physicochemical and cell
620 adhesion properties of chitosan films prepared from sugar and phosphate-containing

621 solutions. *Eur J Pharm Biopharm* 68, 74-81.
622 Chen KL, Wu HC, Chang CH.(2012) Tissue-engineered constructs for urethral regeneration.
623 *Urological Sci* 23, 42-44.
624 Elviri L, Asadzadeh M, Cucinelli R, Bianchera A, Bettini R. (2014) Macroporous chitosan
625 hydrogels: Effect of sulfur on the loading and release behaviour of amino-acid based
626 compounds. *Carbohy Polym* 132, 50-58.
627 Elviri L, Bianchera A, Bergonzi C, Bettini R. (2016) Controlled local drug delivery strategies
628 from chitosan hydrogels for wound healing. *Exp Opin Drug Deliv* 14, 897-908.
629 Elviri L, Foresti R, Bergonzi C, Zimetti F, Marchi C, Bianchera A, Bernini F, Silvestri M,
630 Bettini R. (2017) Highly defined 3D printed chitosan scaffolds featuring improved cell
631 growth. *Biomed Mater* 12,: 045009.
632 Favari E, Zanotti I, Zimetti F, Ronda N, Bernini F, Rotblath GH. (2004) Probucol inhibits
633 ABCA1-mediated cellular lipid efflux. *Arterioscler Thromb Vasc Biol* 24, 2345-2350.

634 Galli C, Parisi L, Elviri L, Bianchera A, Smerieri A, Lagonegro P, Lumetti S, Manfredi
635 E, Bettini R, Macaluso GM. (2016) Chitosan scaffold modified with D-(+) raffinose and
636 enriched with thiol-modified gelatin for improved osteoblast adhesion. *Biomed Mater* 11,
637 015004.
638 Gasperini L, Mano JF, Reis RL. (2014) Natural polymers for the microencapsulation of cells.
639 *J. R. Soc. Interface.* 11, 20140817.
640 Ho MH, Kuo PY, Hsieh HJ, Hsien TY, Hou LT, Lai JY, Wang DM. (2004) Preparation of
641 porous scaffolds by using freeze-extraction and freeze-gelation methods. *Biomater* 25,129-
642 38.
643 Karande TS, Ong JL, Agrawal CM. (2004) Diffusion in musculoskeletal tissue engineering
644 scaffolds: design issues related to porosity, permeability, architecture, and nutrient mixing.
645 *Ann Biomed Eng* 32, 1728-43.
646 Karri V.V., Kuppusamy G., Talluri S.A., Mannemala S.S., Kollipara R., Wadhwani A.D.,
647 Mulukutla S., raju K.R., Malayandi R. (2016) Curcumin loaded chitosan nanoparticles
648 impregnated into collagen-alginate scaffolds for diabetic wound healing Int. Journ Biol.
649 Macromol, 93, 1519-1529
650 Khademhosseini A, Vacanti JP, Langer R.(2009) Progress in tissue engineering. *Sci A*, 300,
651 64–71.
652 Ko YG, Oh HH, Kawazoe N, Tateishi T, Chen G. (2011) Preparation of Open Porous
653 Hyaluronic Acid Scaffolds for Tissue Engineering Using the Ice Particulate Template
654 Method. *J Biomater Sci Polym* 2**2,** 123-38.
655 Kumar MN, Muzzarelli RA, Muzzarelli C, Sashiwa H, Domb AJ. (2004) Chitosan chemistry
656 and pharmaceutical perspectives. *Chem Rev* 104, 6017–84.
657 Liang X, Boppart SA, (2010) Biomechanical Properties of In Vivo Human Skin From
658 Dynamic Optical Coherence Elastography. *IEEE Trans Biomed Eng* 57, 953–959.
659 Macchiarini P.(2008) Clinical transplantation of a tissue-engineered airway *Lancet* 372, 2023-

30.

Mekhail M, Tabrizian M. (2014) Injectable chitosan-based scaffolds in regenerative medicine and their clinical translatability. *Adv Healthc Mater.* 10, 1529-45.

Mizuno K, Yamamura K, Yano K, Osada T, Saeki S, Takimoto N, Sakura T, Nimura Y. (2003) Effect of chitosan film containing basic fibroblast growth factor on wound healing in genetically diabetic mice. *J Biomed Mater Res* 64, 177–81.

Okamoto Y, Minami S, Matsuhashi A, Saimoto H, Shigemasa Y, Tanigawa T, Tanaka Y, Tokura S. (1992) *Advances in chitin and chitosan* Elsevier: New York, .p. 70.

Patil RS, Ghormade VV, Deshpande MV.(2000) Chitinolytic enzymes: an exploration. *Enzyme Microb Technol* 26, 473–83.

Peluso G, Petillo O, Ranieri M, Santin M, Ambrosio L, Calabro D, Avallone B, Balsamo G. (1994) Chitosan-mediated stimulation of macrophage function. *Biomaterials* 15, 1215-20.

Schimming R, Schmelzeisen R. (2004) Tissue-engineered bone for maxillary sinus augmentation. *J Oral Maxillofac Surg* 62,724-9.

Stevens MM, George JH. (2005) Exploring and engineering the cell surface interface. *Science* 310, 1135–1138.

Teng YD Lavik EB, Qu X, Park KI, Ourednik J, Zurakowski D, Langer R, Snyder EY. (2002) Functional recovery following traumatic spinal cord injury mediated by a unique polymer scaffold seeded with neural stem cells. *Proc Natl Acad Sci USA* 99, 3024–3029.

Ueno H, Yamada H, Tanaka I, Kaba N, Matsuura M, Okumura M, Kadosawa T, Fujinaga T. (1999) Accelerating effects of chitosan for healing at early phase of experimental open wound in dogs. *Biomaterials* 20, 1407–14.

Warnke PH (2004) Growth and transplantation of a custom vascularised bone graft in a man. *Lancet* 364, 766-70.

Weigel T, Schinkel G, Lendlein A. (2006) Design and preparation of polymeric scaffolds for tissue engineering. *Expert Rev Med Devices* 3, 835-51.

686 Xue M, Jackson CJ. (2015) Extracellular Matrix Reorganization During Wound Healing and
687 Its Impact on Abnormal Scarring. *Adv Wound Care* 4, 119–136.
688 Yannas IV, Lee E, Orgill DP, Skrabut EM, Murphy GF.(1989). Synthesis and characterization
689 of a model extracellular matrix that induces partial regeneration of adult mammalian skin.
690 *PNAS,* 86, 933-937.
691 Zhang X, Liu Z, Yang Y, Yao Y, Tao Y. (2017) The clinical outcomes of vaginoplasty using
692 tissue-engineered biomaterial mesh in patients with Mayer-Rokitansky-Küster-Hauser
693 syndrome. *International J Surgery* 44, 9-14.
694 Zhao F, Yin Y, Lu WW, Leong JC, Zhang W, Zhang J, Zhang M, Yao K. (2002) Preparation
695 and histological evaluation of biomimetic three-dimensional hydroxyapatite/chitosan–gelatin
696 network composite scaffolds. *Biomaterials* 23, 3227–34.